applied sciences

MDPI

Article

Development of Zirconium-Based Alloys with Low Elastic Modulus for Dental Implant Materials

Minsuk Kim, Seongbin An, Chaeeul Huh and Chungseok Kim *

Department of Materials Science and Engineering, Chosun University, Gwangju 501-759, Korea; okms1304@naver.com (M.K.); tjdqls1134@naver.com (S.A.); gjcodmf@naver.com (C.H.)

* Correspondence: chs2865@chosun.ac.kr; Tel.: +82-6-2230-7197

Received: 15 November 2019; Accepted: 2 December 2019; Published: 4 December 2019

Abstract: The stress-shielding effect is a phenomenon in which the mutual coupling between bones and bio-materials of the human body is loosened due to the difference in elastic modulus, and bone absorption occurs due to the difference in density, which causes a shortening of the life of the material. The purpose of this study is to develop a zirconium-based alloy with low modulus and to prevent the stress-shielding effect. Zr–7Cu–xSn (x = 1, 5, 10, 15 mass%) alloys were prepared by an arc-melting process of pure zirconium, oxygen-free copper, and tin, respectively. The Zr–7Cu–xSn alloy has two phase α-Zr and Zr_2Cu intermetallic compounds. Microstructure characterization was analyzed by microscopy and X-ray diffraction. Corrosion tests of zirconium-based alloys were conducted through polarization tests, and zirconium-based alloys had better corrosion characteristics than other metal bio-materials. In general, the elastic modulus value (14–25 GPa) of the zirconium-based alloy is very similar to the elastic modulus value (15–30 GPa) of the human bone. Consequently, the zirconium-based alloy is likely to be used as a bio-material that negates the effect of stress shielding on human bones.

Keywords: biomaterials; zirconium; dental implant; elastic modulus; alloy design

1. Introduction

Today, metallic materials have good biomechanical properties and suitability for sterilization processes in the biomaterials industry because they have excellent mechanical and corrosion properties. Biomaterials are widely used due to the aging of the population, and metallic materials such as gold, stainless steel, Ti, Co–Cr alloy, and Ni–Ti alloy are used [1–3]. However, the selection of materials for the various components of a biomedical device depends on several factors. First, the metallic implant materials should have good biocompatibility without any side effects. They remain in long-time contact with body fluids and tissues. Therefore, they may cause corrosion or release of alloying elements in the human body, which cause adverse effects [1–4]. Second, they should have good mechanical strength and fatigue resistance to mimic the mechanical properties of bone substitutes [1–3]. For the mechanical strength, most metallic materials have excellent strength properties such as yield strength, tensile/compressive strength, shear strength, fatigue limit for the bone substitutes. However, there is a huge discrepancy of elastic modulus between the present implant metallic materials and human bone. Third, the osteointegration is the direct contact between human bone and the implant materials. For the improvement of osteointegration, many researchers have studied this for a long time and reported many applicable surface treatment techniques such as plasma electrolytic oxidation (PEO) and electrophoretic deposition (EPD) [5–10]. At present, dental materials researchers are also concerned about the contact surface of implants and much research is being done. Recent research shows that surface research is a great help in rehabilitation in the field of dental implants. It has been reported that the application of surface treatments to the alloplastic materials used in rehabilitative

surgery, such as titanium surfaces, has shortened the healing time, especially the time required for osteointegration [11]. These reports can provide better care for clinicians and patients and can be of great help in the field of orthopedic and implant surgery.

The Ti and Ti–6Al–4V alloys are metallic materials that are widely used in dental implants, artificial joints, bone plates, etc. However, many recent studies have shown that both Al and V ions can cause long-term health problems [12,13]. Vanadium has previously been shown to be toxic to humans [14,15]. Element V has been found to react severely with animal tissues, and Al may be associated with nervous system disorders and Alzheimer's disease [12,13]. Moreover, a low elastic modulus is required to transfer the appropriate mechanical stress of the bone to the surrounding bone [2,3]. Low elastic modulus is important for mimicking the bone substitutes to neglect the stress shielding effects due to the unbalanced stress distribution between bone and implant materials [14,15]. The elastic modulus of Ti–6Al–4V alloy is about 110 GPa, which is lower than that of Co–Cr–Mo alloy (230 GPa) [16]. However, Ti–6Al–4V alloys are still significantly higher than the human bone elastic modulus (10–30 GPa) [16]. The difference in elastic modulus between the metallic biomaterials and the human bone causes the stress shielding effect resulting in bone resorption. To solve this stress shielding problem, many new Ti alloys, especially single β-Ti phase alloys, have been developed. Unfortunately, the elastic modulus of most β-type Ti alloys is still high about 60–80 GPa, which is far from the requirement for hard tissue replacement (HTR) [17,18].

The Zr and Zr alloys, which are similar to the Ti and Ti alloys, have excellent biocompatibility and are an advantageous non-toxic metal, are also of interest [19,20]. The Zr is considered a biomechanical advantage because of its low elastic modulus, which minimizes the stress shielding of host bones compared to Ti and Ti alloys [21]. The Zr has also excellent corrosion resistance by the intrinsic oxide film on the surface. Some previous studies on the biological behavior of metals have shown that Zr is an advantageous non-toxic metal similar to Ti and with good biocompatibility [19,20]. It also shows high mechanical strength, high fracture toughness and good corrosion resistance [22–25]. However, so far, research on Zr alloys is extremely rare.

In this study, a Zr–7Cu–xSn alloy was newly designed and manufactured based on Zr, which is considered a potential candidate for orthopedic and implants to neglect the stress shielding effects of metallic implant materials. The Cu element is known as an element that is easy to alloy with other metals and has excellent corrosion resistance. Also, it has long been known to have antimicrobial activity and antibacterial properties. The Sn element is a non-toxic element and has been introduced into biomedical metals [26]. Biocompatibility tests, cytotoxicity tests, and in vitro studies on this designed alloy should be conducted more in the future for clinical and surgical applications.

2. Experimental Details

2.1. Alloy Manufacturing

Zirconium-based alloys were prepared using pure zirconium (99.9 mass%), oxygen-free copper (99.9 mass%), and tin (99.99 mass%) using the arc-melting process in an Ar atmosphere. The types and chemical compositions of designed Zr–7Cu–xSn alloys are listed in Table 1.

Table 1. Chemical compositions of the alloys used in this study (in wt%).

Zr–7Cu–xSn	1%	5%	10%	15%
Zr	92	88	83	78
Cu	7	7	7	7
Sn	1	5	10	15

2.2. X-ray Diffraction (XRD) Test

In order to observe the change in the crystal phase structure of the test specimens, it was carried out using an X-ray diffractometer (XRD, Rigaku: X'pert PRO MRD) with a 2θ scan with a holding time

of 1 s at a scan interval of 0.02 degrees from 30 degrees to 80 degrees. X-rays were set at a tube voltage of 40 kV and a current of 30 mA under CuKα conditions.

2.3. Microstructure Characterization

The microstructure of the alloys was observed by microscopes. The test specimens were prepared by mechanical polishing from 400 grit to 4000 grit using emery paper, and the micropolishing operation was performed using an alumina paste (0.05 μm). Thereafter, chemical etching was performed for about 6 s using 45 mL of distilled water, 45 mL of nitric acid, and 10 mL of hydrofluoric acid (Dist water 45 mL + Nitric acid 45 mL + Hydrofluoric acid 10 mL). Using the prepared specimens, the microstructure was observed by using an optical microscope (OM, Carl Zeiss: Axio Vert. A1, GER), scanning electron microscope (SEM, Seron: AIS2000 C, KOR).

2.4. Mechanical Property Test

The compression test was performed using a universal testing machine (UTM, Shimadzu: AG-20 Knx, JAP) to measure the mechanical properties, compressive strength, yield strength and elastic modulus of the specimen. The compression test specimen was prepared by a wire cutting with 3 mm × 3 mm × 6 mm. The test was carried out at an initial strain of 1 mm/min at room temperature to obtain a stress–strain curve. The hardness of the alloy was measured using a Vickers hardness tester (Shimadzu: HMV-G21, JAP) with a hold time of 5 s under a 19.61 N load.

2.5. Electrochemical Corrosion Measurement

Corrosion tests were performed using normal saline as the electrolyte, similar to the human body condition. The emery paper was used up to 4000 grit, and the specimen was prepared using the alumina paste (0.05 μm). Potential polarization measurements were performed from −0.5 V to 1.5 V with a scan rate of 1 mV/s.

3. Results and Discussion

3.1. Microstructure and Phase Observation

Figure 1 shows the XRD profile of the Zr–7Cu–xSn alloys. In the diffraction peak, a high Zr_2Cu diffraction peak was observed around 2θ = 37°, and the addition of Sn did not change the crystalline structure of Zr. However, as the Sn content increased, the peak intensity of the α-Zr phase lowered. Figure 2 shows the microstructural photograph of Zr–7Cu–xSn alloy. The α-Zr phase and dark gray phase Zr_2Cu intermetallic compounds were observed. As Sn content increases, the Zr_2Cu grows and changes from dendritic structure to large plate phase as shown in Figure 2d.

Figure 3 shows a scanning electron microstructural photograph of each composition. The lamellar structure in the Zr alloy can be clearly seen, which is identified to be α-Zr + Zr_2Cu eutectic structure. The Zr_2Cu eutectic phase is circular around the interface. Based on the Zr-Cu binary phase diagram [27], the intermetallic phase Zr_2Cu is generated when the Cu content is low. These Zr_2Cu phases can be classified into two phases: precipitated phase (formed due to decrease in the solubility of Cu and Zr as the temperature decreases) and eutectoid phase (formed at temperatures below 820 °C). As the solubility of Cu atoms decreases as the temperature decreases, they dissolve into β-Zr, and Cu atoms diffuse into the grain boundary region to form a Zr_2Cu phase [27]. According to the Zr-Sn binary phase diagram, Sn raises the α→β transformation temperature and it has a solid solubility of 8.3 wt% in α-Zr [28]. Therefore, even if a small amount of Sn is added, the structure of Zr does not change and Sn is dissolved in Zr.

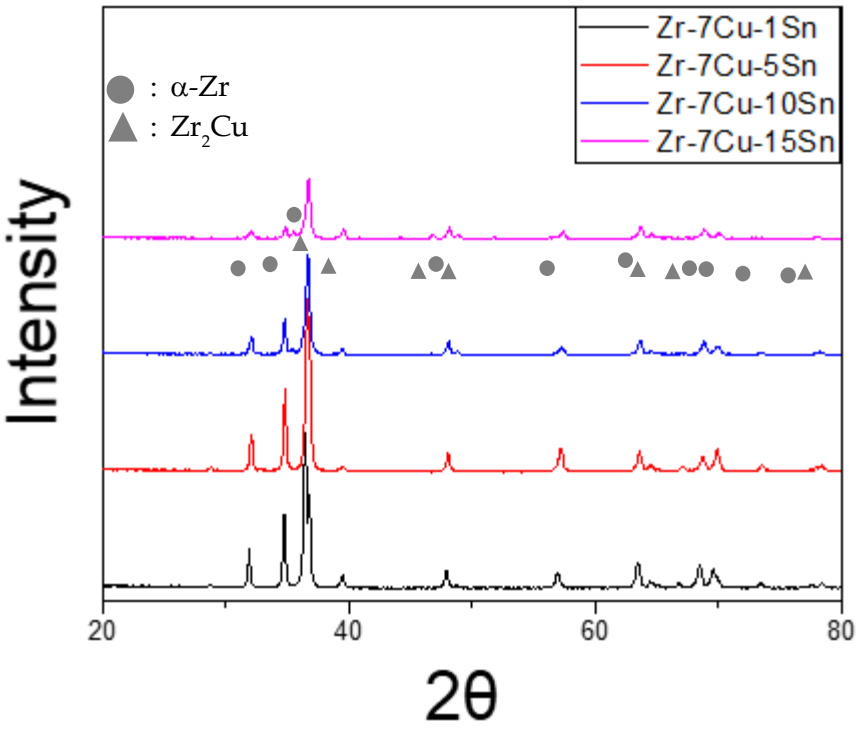

Figure 1. X-ray diffraction (XRD) profiles of Zr–7Cu–xSn (x = 1, 5, 10, 15 wt%).

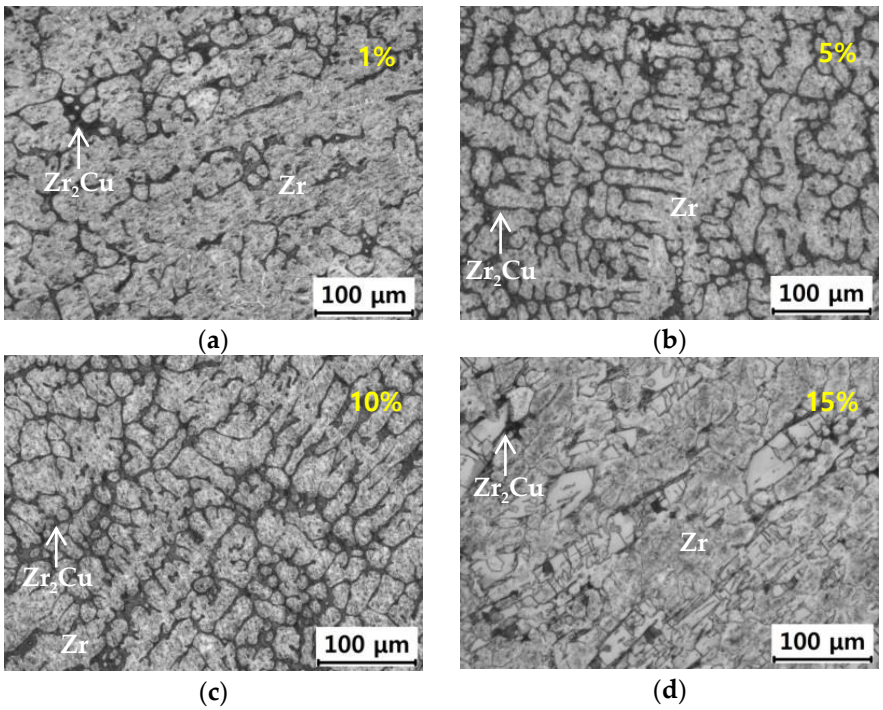

Figure 2. Optical microscopy (OM) micrographs of Zirconium-base alloys; Zr–7Cu–xSn (x = 1, 5, 10, 15 wt%): (**a**) Zr-7Cu-1Sn, (**b**) Zr-7Cu-5Sn, (**c**) Zr-7Cu-10Sn, (**d**) Zr-7Cu-15Sn.

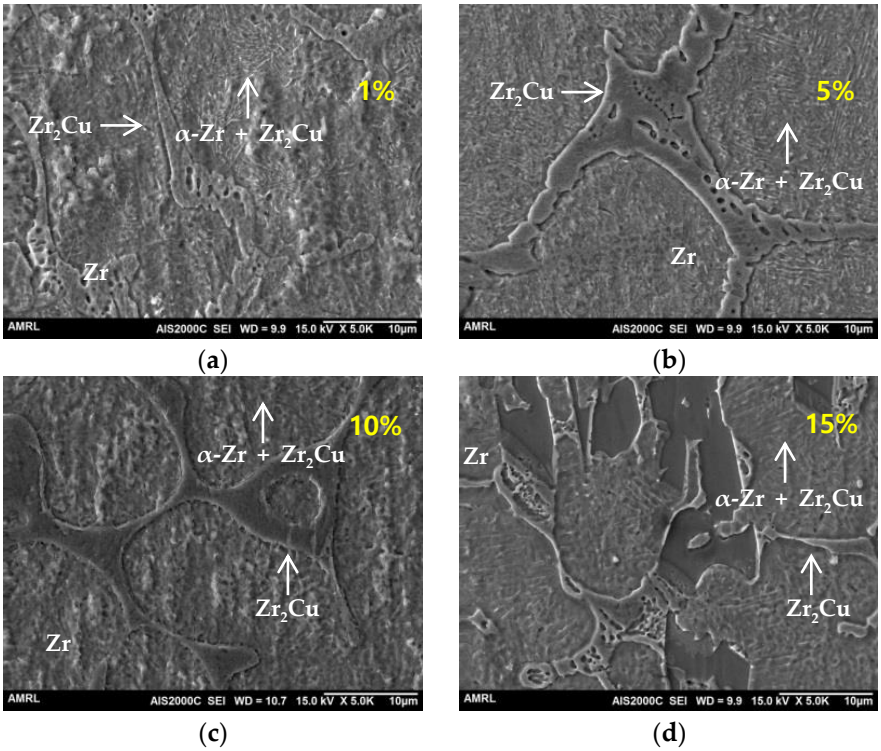

Figure 3. Scanning electron microscopy (SEM) micrographs of Zirconium-base alloys; Zr–7Cu–xSn (x = 1, 5, 10, 15 wt%): (**a**) Zr–7Cu–1Sn, (**b**) Zr–7Cu–5Sn, (**c**) Zr–7Cu–10Sn, (**d**) Zr–7Cu–15Sn.

3.2. Mechanical Properties

To investigate the mechanical properties, the stress–strain curve of Zr–7Cu–xSn alloys through a compression test is shown in Figure 4. The yield strength and compressive strength increase and the ductility decrease as the Sn content increases. This can be seen as a solid solution strengthening effect in the Zr–7Cu–xSn ternary alloys. As already discussed in the microstructural observation, the Zr_2Cu intermetallic phase grows and changes from dendritic structure to large plate phase as shown in Figure 2d. This Zr_2Cu intermetallic phase is a harder and more brittle phase than the matrix α-Zr. In addition to solid solution strengthening, the strength of ternary alloys increased with the Zr_2Cu phase. Therefore, it can be inferred that the yield strength and plastic deformation of the Zr–7Cu–xSn alloy are affected by Sn. In addition, the elastic modulus, hardness and elastic energy increase with Sn content. These mechanical test results are shown in Table 2.

As shown in Figure 2 the secondary phase Zr_2Cu intermetallic compound is uniformly distributed throughout, resulting in a secondary phase strengthening effect. However, the Zr_2Cu phase increases in size, leading to a decrease in ductility. Therefore, in order to obtain an ideal Zr–7Cu–xSn alloy, the Sn content must be within 15%. The yield strength of Zr–7Cu–xSn alloys is in the range of 610–970 MPa, and compressive strength is in the range of 860–1200 MPa, which is higher than most metallic biomaterials such as Ti alloys [29]. The elastic modulus of Zr–7Cu–xSn alloys is in the range of 14–18 GPa. This is similar to the elastic modulus value of human bones (15–30 GPa) and much lower than that of Ti biomaterials being studied [30]. Therefore, zirconium-based alloys are well suited as implant materials to neglect the stress-shielding effect.

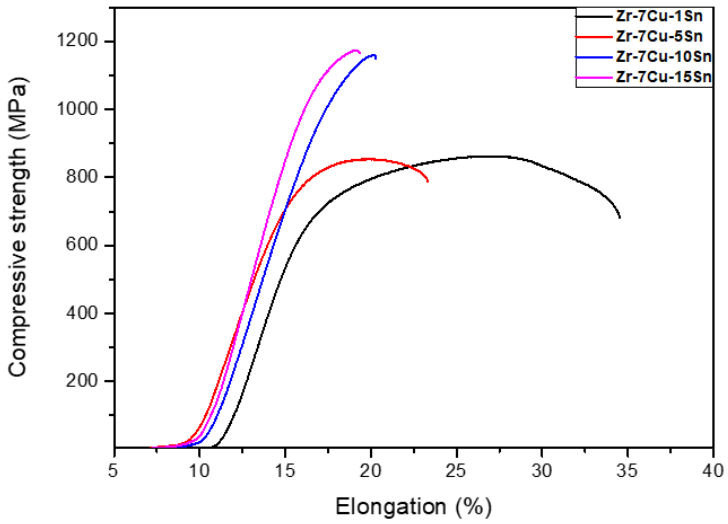

Figure 4. Compressive stress–strain Curves of Zr–7Cu–xSn (x = 1, 5, 10, 15 wt%).

Table 2. Mechanical properties of Zr–7Cu–xSn (x = 1, 5, 10, 15 wt%).

Zr–7Cu–xSn	1%	5%	10%	15%
Compressive strength (MPa)	861	853	1159	1173
Yield strength (MPa)	614	652	900	969
Elongation (%)	34.5	23.3	20.2	19.3
Elastic modulus (GPa)	14.7	14.4	15.6	17.8
Hardness (Hv)	247	293	362	369
Elastic energy (MJ/m^3)	14.4	16.4	28	28.8

3.3. Elastic Modulus Measurement

The metal biomaterials used for implants require high strength and low modulus. The formula of elastic energy can be expressed as follows.

$$\delta_e = 1/2\sigma_y \varepsilon_e = \sigma^2{}_y/2E \quad (1)$$

where δe is the elastic energy, σ_y is the yield strength, ε_e is the elastic deformation and E is an elastic modulus.

According to Equation (1), the elastic energy of Zr–7Cu–xSn alloys is possibly calculated, and the results are depicted in Table 2. The elastic energy increased high with Sn addition. Over Zr–7Cu–10Sn alloy, it does not increase a little. Most of all, the elastic energy of Zr–7Cu–xSn alloys is the range of 14.4~28.8 MJ/m^3, which is higher than that of general Ti-based biomaterials [31]. From these results of this study, the developed Zr–7Cu–xSn alloys may endure the higher deformation than the commercial biomaterials. In addition, the press-fit phenomenon occurring at implant insertion induces biomechanical effects in the bone tissues, which ensure implant primary stability [32]. In this point of view, this Zr-Cu-Sn ternary alloy has the same level of elastic modulus with human bone. Therefore, we can expect that the press-fit phenomenon may be reduced compared with the present biomaterials.

3.4. Corrosion Measurement

Figure 5 shows the potential polarization curves of Zr–7Cu–xSn alloys tested in normal saline. Current density (Icorr) and corrosion potential (Ecorr) were determined by a Tafel extrapolation. Their average values are shown in Table 3. Zr–7Cu–xSn alloys were found to be insignificant depending on the composition. However, current density values are lower than titanium alloys [33]. Therefore,

Zr–7Cu–xSn alloys are best suited for biomaterials because they have better corrosion resistance than Ti alloys.

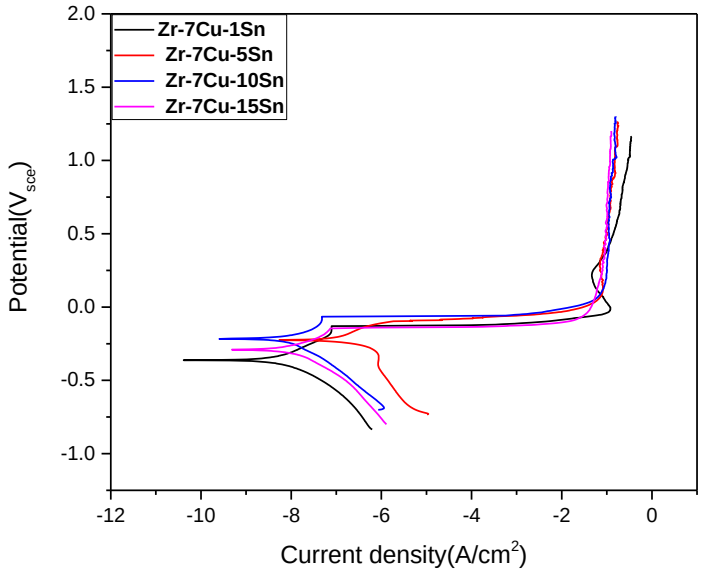

Figure 5. Potential polarization curves of Zr–7Cu–xSn (x = 1, 5, 10, 15 wt%).

Table 3. Average value of current density and corrosion potential of Zr–7Cu–xSn (x = 1, 5, 10, 15 wt%).

Zr–7Cu–xSn	1%	5%	10%	15%
Icorr [μA/cm^2]	0.00065	0.0039	0.00090	0.0031
Ecorr [mV]	−360.8	−226.3	−215.5	−288.7

4. Conclusions

The Zr–7Cu–xSn alloys were designed and manufactured for the first time to develop a new biomaterial with high strength, elasticity similar to human bone, and good corrosion resistance. This leads to the following conclusion.

(1) In the Zr–7Cu–xSn alloys, Zr_2Cu, an intermetallic compound was distributed along grain boundaries. As the Sn content increases, the Zr matrix decreases and the Zr_2Cu phase coarsened to confirm solid solution strengthening.

(2) The compression test was performed to obtain the stress–strain curves of the alloys. The compressive strength of the Zr–7Cu–xSn alloy was in the range of 860–1200 MPa. The elastic modulus was obtained in the range of 14–18 GPa. It is possibly considered zirconium-based alloys are well suited as implant materials to neglect the stress-shielding effect.

(3) A polarization test was conducted to measure the corrosion behavior of Zr–7Cu–xSn alloys. The addition of Sn lowered the current density of Zr, and the average value of the current density of Zr–7Cu–xSn alloy was about 0.0100 μA/cm^2. Therefore, it can be regarded as a biomaterial having good corrosion resistance.

Author Contributions: M.K., S.A., and C.H. carried out the experiments. M.K. wrote the manuscript with support from S.A. and C.H. C.K. conceived the original idea and supervised the project.

Funding: This research received no external funding.

Acknowledgments: This research was supported by the National Research Foundation of Korea (NRF) funded by the Ministry of Education (NO. 2017R1D1A3B03028681).

Conflicts of Interest: The authors declare no conflict of interest.

References

1. Miura, K.; Yamada, N.; Hanada, S.; Jung, T.-K.; Itoi, E. The bone tissue compatibility of a new Ti–Nb–Sn alloy with a low Young's modulus. *Acta Biomater.* **2011**, *7*, 2320–2326. [CrossRef] [PubMed]
2. Cremasco, A.; Andrade, P.N.; Contieri, R.J.; Lopes, E.S.N.; Afonso, C.R.M.; Caram, R. Correlations between aging heat treatment, ω phase precipitation and mechanical properties of a cast Ti–Nb alloy. *Mater. Des.* **2011**, *32*, 2387–2390. [CrossRef]
3. Guo, Q.; Zhan, Y.; Mo, H.; Zhang, G. Aging response of the Ti–Nb system biomaterials with β-stabilizing elements. *Mater. Des.* **2010**, *31*, 4842–4846. [CrossRef]
4. Cicciù, M.; Fiorillo, L.; Herford, A.S.; Crimi, S.; Bianchi, A.; D'Amico, C.; Laino, L.; Cervino, G. Bioactive Titanium Surfaces: Interactions of Eukaryotic and Prokaryotic Cells of Nano Devices Applied to Dental Practice. *Biomedicines* **2019**, *7*, 12. [CrossRef] [PubMed]
5. Ha, J.-Y.; Tsutsumi, Y.; Doi, H.; Nomura, N.; Kim, K.-H.; Hanawa, T. Enhancement of calcium phosphate formation on zirconium by micro-arc oxidation and chemical treatments. *Surf. Coat. Technol.* **2011**, *205*, 4948–4955. [CrossRef]
6. Sundararajan, G.; Rama Krishna, L. Mechanisms underlying the formation of thick alumina coatings through the MAO coating technology. *Surf. Coat. Technol.* **2003**, *167*, 269–277. [CrossRef]
7. Sreekanth, D.; Rameshbabu, N.; Venkateswarlu, K. Effect of various additives on morphology and corrosion behavior of ceramic coatings developed on AZ31 magnesium alloy by plasma electrolytic oxidation. *Ceram. Int.* **2012**, *38*, 4607–4615. [CrossRef]
8. Venkateswarlu, K.; Rameshbabu, N.; Sreekanth, D.; Bose, A.C.; Muthupandi, V.; Babu, N.K.; Subramanian, S. Role of electrolyte additives on in-vitro electrochemical behaviour of micro arc oxidized titania films on Cp Ti. *Appl. Surf. Sci.* **2012**, *258*, 6853–6863.
9. Yerokhin, A.L.; Nie, X.; Leyland, A.; Matthews, A.; Dowey, S.J. Plasma electrolysis for surface engineering. *Surf. Coat. Technol.* **1999**, *122*, 73–93. [CrossRef]
10. Zhang, B.; Kwok, C.T. Hydroxyapatite-anatase-carbon nanotube nanocomposite coatings fabricated by electrophoretic codeposition for biomedical applications. *J. Mater. Sci. Mater. Med.* **2011**, *22*, 2249–2259. [CrossRef]
11. Xu, R.; Hu, X.; Yu, X.; Wan, S.; Wu, F.; Ouyang, J.; Deng, F. Micro-/nano-topography of selective laser melting titanium enhances adhesion and proliferation and regulates adhesion-related gene expressions of human gingival fibroblasts and human gingival epithelial cells. *Int. J. Nanomed.* **2018**, *13*, 5045–5057. [CrossRef] [PubMed]
12. Zhou, Y.L.; Niinomi, M.; Akahori, T. Effects of alloying additions on mechanical properties of Ti–Hf and Ti–Ta alloys. *Mater. Sci. Eng. A* **2004**, *384*, 92–101. [CrossRef]
13. Rao, S.; Ushida, T.; Tateishi, T.; Okazaki, Y.; Asao, S. Effect of Ti, Al, and V ions on the relative growth rate of fibroblasts (L929) and osteoblasts (MC3T3-E1) cells. *Bio-Med. Mater. Eng.* **1996**, *6*, 79–86. [CrossRef] [PubMed]
14. Rae, T. The toxicity of metals used in orthopaedic prostheses. An experimental study using cultured human synovial fibroblasts. *J. Bone Jt. Surg. Br. Vol.* **1981**, *63-B*, 435–440. [CrossRef]
15. Hallab, N.J.; Vermes, C.; Messina, C.; Roebuck, K.A.; Glant, T.T.; Jacobs, J.J. Concentration-and composition-dependent effects of metal ions on human MG-63 osteoblasts. *J. Biomed. Mater. Res.* **2002**, *60*, 420–433. [CrossRef]
16. Long, M.; Rack, H.J. Titanium alloys in total joint replacement—A materials science perspective. *Biomaterials* **1998**, *19*, 1621–1639. [CrossRef]
17. Nag, S.; Banerjee, R.; Fraser, H. A novel combinatorial approach for understanding microstructural evolution and its relationship to mechanical properties in metallic biomaterials. *Acta Biomater.* **2007**, *3*, 369–376. [CrossRef]
18. Niinomi, M. Recent metallic materials for biomedical applications. *Metall. Mater. Trans. A* **2002**, *33*, 477–486. [CrossRef]
19. Niinomi, M. Recent titanium R&D for biomedical applications in japan. *JOM* **1999**, *51*, 32–34.
20. Saldana, L.; Mendezvilas, A.; Jiang, L.; Multigner, M.; Gonzalezcarrasco, J.; Perezprado, M.; Gonzalezmartin, M.; Munuera, L.; Vilaboa, N. In vitro biocompatibility of an ultrafine grained zirconium. *Biomaterials* **2007**, *28*, 4343–4354. [CrossRef]

21. Yan, Y.; Han, Y. Structure and bioactivity of micro-arc oxidized zirconia films. *Surf. Coat. Technol.* **2007**, *201*, 5692–5695. [CrossRef]
22. Wen, C.E.; Yamada, Y.; Hodgson, P.D. Fabrication of novel TiZr alloy foams for biomedical applications. *Mater. Sci. Eng. C* **2006**, *26*, 1439–1444. [CrossRef]
23. Okazaki, Y.; Rao, S.; Tateishi, T.; Ito, Y. Cytocompatibility of various metal and development of new titanium alloys for medical implants. *Mater. Sci. Eng. A* **1998**, *243*, 250–256. [CrossRef]
24. Niinomi, M. Fatigue performance and cyto-toxicity of low rigidity titanium alloy, Ti–29Nb–13Ta–4.6Zr. *Biomaterials* **2003**, *24*, 2673–2683. [CrossRef]
25. Inoue, A. Stabilization of metallic supercooled liquid and bulk amorphous alloys. *Acta Mater.* **2000**, *48*, 279–306. [CrossRef]
26. Niinomi, M. Recent research and development in titanium alloys for biomedical applications and healthcare goods. *Sci. Technol. Adv. Mater.* **2003**, *4*, 445–454. [CrossRef]
27. Okamoto, H. Cu-Zr (Copper-Zirconium). *J. Phase Equilib. Diffus.* **2012**, *33*, 417–418. [CrossRef]
28. Okamoto, H. Sn-Zr (Tin-Zirconium). *J. Phase Equilib. Diffus.* **2010**, *31*, 411–412. [CrossRef]
29. Niinomi, M. Mechanical properties of biomedical titanium alloys. *Mater. Sci. Eng. A* **1998**, *243*, 231–236. [CrossRef]
30. Niinomi, M.; Nakai, M. Titanium-Based Biomaterials for Preventing Stress Shielding between Implant Devices and Bone. *Int. J. Biomater.* **2011**, *2011*, 1–10. [CrossRef]
31. Li, C.; Zhan, Y.; Jiang, W. β-Type Ti–Mo–Si ternary alloys designed for biomedical applications. *Mater. Des.* **2012**, *34*, 479–482. [CrossRef]
32. Natali, A.N.; Carniel, E.L.; Pavan, P.G. Investigation of viscoelastoplastic response of bone tissue in oral implants press fit process. *J. Biomed. Mater. Res.* **2009**, *91*, 868–875. [CrossRef] [PubMed]
33. Lu, J.; Zhao, Y.; Niu, H.; Zhang, Y.; Du, Y.; Zhang, W.; Huo, W. Electrochemical corrosion behavior and elasticity properties of Ti–6Al–xFe alloys for biomedical applications. *Mater. Sci. Eng. C* **2016**, *62*, 36–44. [CrossRef] [PubMed]